Functional mechanical attributes of natural and synthetic gel-based scaffolds in tissue engineering: strain-stiffening effects on apparent elastic modulus and compressive

FUNCTIONAL MECHANICAL ATTRIBUTES OF NATURAL AND SYNTHETIC GEL-BASED SCAFFOLDS IN TISSUE ENGINEERING: STRAIN-STIFFENING EFFECTS ON APPARENT ELASTIC MODULUS AND COMPRESSIVE TOUGHNESS

Alessandro Schiavi[a]*, Rugiada Cuccaro[a], Adriano Troia[a]

[a] *INRiM – Istituto Nazionale di Ricerca Metrologica, Strada delle Cacce 91,10135 Torino, Italy*

* Corresponding author. Tel: +39 0113919916, Fax: +39 0113919621

E-mail addresses: a.schiavi@inrim.it (A. Schiavi), r.cuccaro@inrim.it (R. Cuccaro), a.troia@inrim.it (A. Troia)

Highlights • Strain-stiffening effects, apparent elastic modulus, compressive toughness, natural and synthetic gel-based scaffolds.

Abstract

The accurate identification and determination of apparent elastic modulus and toughness, as well as other functional mechanical attributes of artificial tissues, are of paramount importance in several fields of tissue science, tissue engineering and technology, since biomechanical and biophysical behavior is strongly linked to biological features of the medical implants and tissue-engineering scaffolds. When soft or ultra-soft materials are investigated, a relevant dispersion of elastic modulus values can be achieved, due to the strain-stiffening effects, inducing a typical non-linear behavior of these materials, as a function of strain-range. In this short communication, the Apparent elastic modulus strain-range dependence is estimated from a segmentation of the strain stiffening curve, and the related compressive toughness is investigated and discussed, based on experimental evidence, for 6 different kinds of gels, used for artificial tissue fabrication; experimental results are compared to mechanical properties of native human tissues.

1. Introduction

Natural and synthetic gels are easily moldable in three-dimensional structural matrices and scaffolds able of giving rise to tissues with analogous mechanical properties of native human tissue [1 – 8], from the microscale (cellular scale) [9 – 10] up to the macroscale (organ scale) [11 – 12]. Gel-based scaffolds, due to the ability to tailor mechanical behavior to mimic natural tissues, are extensively applied as biomaterials over a broad range of both *in-vitro* and *in-vivo* applications, such as tissue regeneration [13], tissue restoring/replacing [14], drug delivery [15], vascularization [16], and simultaneous seeding of multiple cells [17]; gel-based matrices are widely used for wound healing and repair [18 – 20], as well as for cosmetic applications [21 – 23]. Mechanical properties of these biomimetic structures, beyond being related to biological and biomechanical features, such as biocompatibility, biodegradability, and functionality of medical implants [24 – 27], significantly influence adhesion, growth, and differentiation of cells: biomechanical cues of tissue-engineering

scaffolds, integrated with biomolecular cues, allow to maintain pluripotency or to induce differentiation in stem cells [28]. Moreover, the elastic properties and the toughness of gel-based matrices are effective representatives of typical largescale deformations of human organ tissues, up to traumatic failures and lacerations [29 -32]. As a consequence, an accurate characterization of mechanical properties, in terms of apparent elastic modulus E and toughness W_c of artificial tissues, allows evaluating with reliability the technical performances, biological behaviors, or other related phenomena associated with them.

Strictly speacking, since the Young's Modulus value cannot be univocally identified for soft or ultra-soft artificial tissues, due to the strain-stiffening effects [33], inducing a non-linear elastic behavior [34], the elastic response to mechanical stresses is defined in terms of apparent elastic modulus. Experimental procedures and measurement methods can affect experimental results [35 – 37], as well as temperature and strain rate [38]. As a result, the elastic properties of soft artificial tissues should be expressed with well-defined boundaries conditions. In this paper, based on accurate experimental evidence, apparent elastic modulus and compressive toughness (within strain-stiffening effects) of soft and ultra-soft gel-based matrices, are investigated and discussed, as a function of the strain-range; experimental results are compared with data collected in the relevant literature, and an extensive (not exhaustive) bibliographic review is provided as a reference for both materials and methods here discussed.

Functional mechanical attributes of native human tissues have been investigated since the first decades of the last century [39]. Experimental observations, based on tensile and compressive tests on muscles, skin, tendons, and other soft tissues, often showed a very peculiar behavior (sometimes recognized as leather-like behavior) with a "stretched-elastic" response, up to the laceration point [40 – 48]. As schematically shown in Figure 1, a native tissue shows exponential relations between stress and strain, both in compression and tension, due to the inherent responsiveness of the elastin-collagen network to recover and compensate deformations [49].

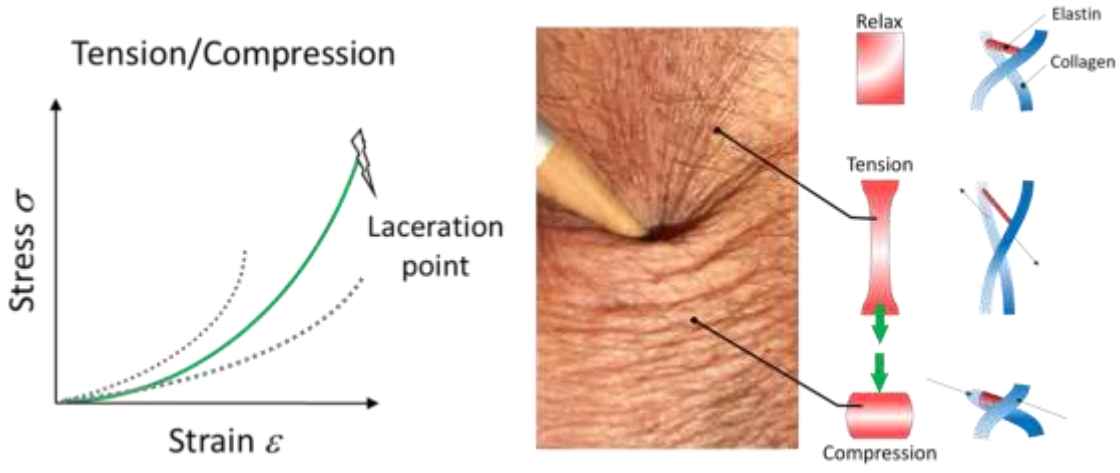

Figure 1. The stretched-elastic responses in tension and compression of human skin and an idealization of the corresponding elastin-collagen network deformations.

According to the literature, as shown in Figure 2, for native soft tissues and organs apparent elastic modulus E ranges on average from 0.1 kPa up to 500 kPa [50, 51], depending on the function and location of the tissues.

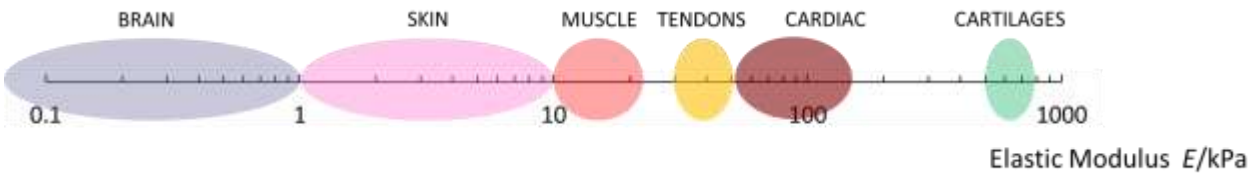

Figure 2. Typical ranges of apparent elastic modulus of several native soft human tissues.

In general terms, as shown in the following sections, three-dimensional structural gel-based matrices and scaffolds opportunely molded, allow to mimic mechanical behaviors in compression, and the related elastic and tough responses [52 – 54], very close to the natural behavior of native human tissues [55 – 61].

2. Materials and experimental method

2.1 Natural and synthetic gel-based tissues

Six gel-based samples, used as tissue-engineering scaffolds, have been molded in cylindrical shape samples (diameter 50 mm, height 30 mm), except Sample #6 (diameter 30 mm, height 5 mm), to perform the unconfined bulk compression tests. The elastic response of the examined gel-based samples is defined in terms of apparent elastic modulus and compressive toughness in the macroscale range. As a polymeric matrix of tissue-engineering scaffolds, three polysaccharides, two synthetic polymers, and one ECM-gel have been used, respectively: Agar [62], Carrageenan [63], Gellan Gum [64], Polyvinylalcohol (PVA) [65], Polyacrylamide (PAA) [66], and Extracellular matrix made from Engelbreth-Holm-Swarm (EHS) sarcoma of *mus musculus* [67]. In Table 1, the sample *id* number, the gel-based typology, and the chemical composition and description, are shown.

Table 1. The gel-based samples analyzed in this investigation.

Sample #	Gel-based Typology	Chemical composition
# 1	Agar	*natural, linear polysaccharide, soft gel in aqueous solution*
# 2	k-Carrageenan	*natural, linear polysaccharide, rigid gel in aqueous solution*
# 3	Gellan Gum	*natural, anionic polysaccharide, hard gel in presence of divalent ions in aqueous solution*
# 4	Polyvinylalcohol	*Synthetic, vinyl polymer, highly elastic hydro-gel after freeze thaw cycles of aqueous solutions*
# 5	Polyacrylamide	*Synthetic, linear polymer of acrylamide, soft water absorbent gel*

# 6	ECM-gel	*Natural, network of extracellular macromolecules forming hard or soft gel depending on composition and concentration in cell culture media*

Agar (2 % in weight) sample has been prepared by dissolving Agar in water and heating up to 80 °C for 5 min. Then it was poured into the mold while cooling.

Carrageenan is a linear sulphated polysaccharide extracted from red edible seaweeds. In our experiments, k-Carrageenan (2 % in weight) has been dissolved in water then heated up to 80 °C for 5 min and poured into the mold while cooling.

Gellan Gum is a more complex polysaccharide, which consists of two residues of D-glucose and one of each residue of L-rhamnose and D-glucuronic acid. In this case, the electrostatic crosslinking mechanism, using divalent ions, has been exploited. A Gellan Gum (2 % in weight) has been prepared by dissolving Gellan Gum in water and heating up to 70 °C, once the solution was homogenous it has been poured into the mold and left cooling. Then the soft gel was dipped into 1 M solution of $CaCl_2$ overnight to increase the hardness of the sample by the crosslinking action of Calcium ions

Polyvinylalcohol (PVA) sample has been prepared to exploit the freezing–thaw technique using a PVA (98 kDa). A 5 % in weight solution has been dissolving PVA in water and heating up to 80 °C for 5 min. Once the solution was homogenous it was poured into the mold and then it was kept at - 25 °C for 18 h. The cycle has been repeated twice.

Polyacrylamide sample has been prepared by one of the methods to polymerize acrylamide. Briefly: 0.526 gr of N, N'-methylene-bis-acrylamide has been dissolved into 100 ml of an aqueous solution of acrylamide (10 % in weight). Then 1 ml of ammonium persulfate (10 % in weight) has been added to the solution and 0.5 ml of Tetramethylethylenediamine has been used to initiate the polymerization reaction. By using this monomer/cross-linking agent ratio, we estimate that the sample has a cross-linking density of about 3-4 mole/m^3, as reported in [68]. The solution was then poured into the mold and it will be hereafter referred to as PAA.

Biological supports based on extracellular matrix (ECM) are generally derived by “decellularizing” intact tissues, so the resulting ECMs are made up of the structural and functional molecules that characterize the native tissue such as collagen, laminin, fibronectin, growth factors, glycosaminoglycans, glycoproteins, and proteoglycans. For the study of cell proliferation mechanisms, these matrices are usually diluted in a 1:1 ratio in culture solutions (Dulbecco’s Modified Eagle’s Medium). However, since in our testing measurment set-up the sample have to retain the shape for its own weight and the action of the deforming plate for these trials the elastic properties of the concentrated ECM gel (ECM gel from Engelbreth-Holm-Swarm murine sarcoma conc. 8-12 mg/ml fro Sigma Aldrich) samples have been studied. ECM is usually stored at a temperature of -25 °C, so the samples have been thawed 24 hours before use and then poured ina smaller cilindircal mould (dimenter 4 cm, height 1.5 cm).

2.2 Experimental system and test procedure

The functional mechanical attributes, in terms of apparent elastic modulus E and compressive toughness W_c, of the above-mentioned tissue-engineering scaffolds, have been determined from the stress-strain diagrams of the engineering uniaxial compression test until breaking. Measurements have been carried out at a constant temperature of 20 °C with a slow constant strain rate of $3 \cdot 10^{-3}\ s^{-1}$ (i.e., 0.1 $mm \cdot s^{-1}$ of deformation rate). Samples have been placed between two aluminum parallel plates and have been compressed by a linear displacement acting perpendicularly on the upper surface of gels. Parallel plates have been lubricated with a thin layer of glycerine to prevent any friction between samples and plates and also to guarantee a homogeneous uniaxial deformation. Measurements have been carried out in displacement control and the resulting force has been measured downstream, as detailed described in [36]. The linear displacement has been measured with an accuracy of 1 μm (resolution 0.1 μm) and the resulting forces have been measured with an accuracy of 10 mN (resolution of 1 mN). A picture of the complete experimental setup, in the climatic cell, is showed in Figure 3.

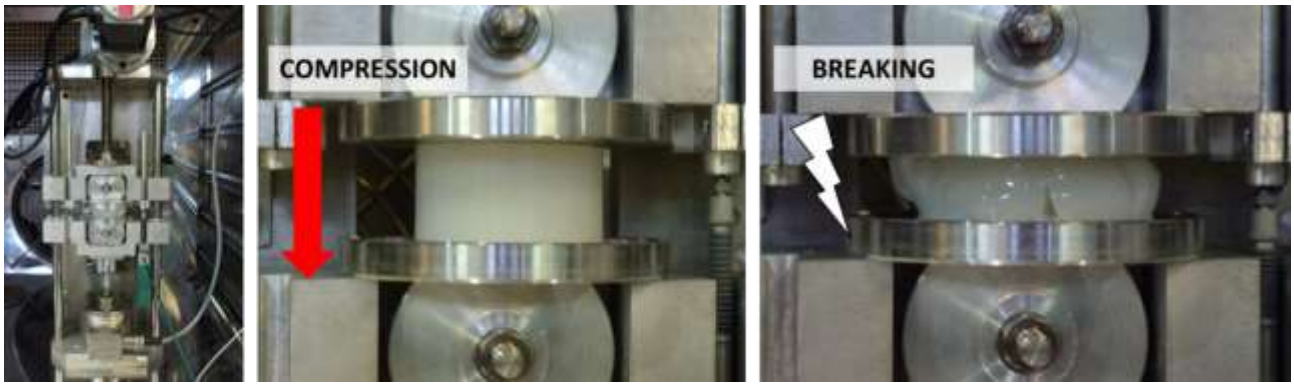

Figure 3. Experimental device to perform uniaxial unconfined compression test and details of a gel-based sample compressed until breaking.

2.3 Mechanical models

Experimentally, apparent elastic modulus E is determined in compression from the ratio between the incremental stress and the incremental strain applying the classical Hooke's law at a constant strain rate, as shown below:

$$E = \frac{\Delta\sigma}{\Delta\varepsilon} = \frac{F}{A} \cdot \frac{l_0}{\Delta l} \quad (1)$$

where E is the apparent elastic modulus (Pa), $\Delta\sigma$ incremental compressive stress (Pa), $\Delta\varepsilon$ incremental compressive strain (dimensionless), F compression force (N), A surface area of the sample (m^2), on which the force acts, l_0 initial thickness of the sample (m), and Δl is the occurring deformation (m) due to the application of F within the strain range in which the sample under investigation shows an elastic behavior.

The compressive toughness W_c (kJ·m^{-3}) is determined by calculating the area under the stress-strain curve, by taking into account the stored energy, in terms of work-of-fracture during compression test, as follows:

$$W_c = \int_0^{\varepsilon_q} \sigma \cdot d\varepsilon \quad (2)$$

Where ε_q is the extensibility, defined as the maximum value of strain, within the stretched-elastic region. Extensibility ε_q corresponds to yield strain value ε_y if the material shows a ductile-like behavior, or breaking strain value ε_b if the material shows brittle-like behavior; the corresponding stress value σ_q defines the strength of the material at the breaking or yielding point. According to these boundary conditions, the compressive toughness W_c quantitatively corresponds to the modulus of resilience.

To accurately interpolate the experimental data and to build suitable functions to be integrated, as shown in relation (2), the stress-strain curve is fitted with cubic polynomial functions, based on the closest to 1 value of the coefficient of determination, as follows:

$$\sigma(\varepsilon) = a \cdot \varepsilon^3 + b \cdot \varepsilon^2 + c \cdot \varepsilon + d \quad (3)$$

Where *a*, *b*, *c*, and *d* are fitting parameters.

In equation (1), the quantity *E* is determined from the linear best-fit of the measured stress-strain curve: the angular coefficient supplies elastic (or storage) modulus value. Nevertheless, due to the peculiar elastic response of gel-based, a stress-strain "stretched" curve occurs in compression, as shown in Figure 2 and from relation (3); namely, non-linear behavior is properly due to the strain-stiffening. Thus apparent elastic modulus can be determined more accurately for only discrete intervals of strain-range $\Delta\varepsilon_i$, as similarly described in [69] and schematically depicted in Figure 4. The apparent elastic modulus values are determined as a function of strain-ranges $\Delta\varepsilon_i$ (with a constant width) to reduce the differential between secant and curve below. By way of example, apparent elastic modulus values E_1 and E_2, determined in two different ranges of strain ($\Delta\varepsilon_1$ between 10 % and 20 % of strain, and $\Delta\varepsilon_2$ between 30 % and 40 %), show two very different slopes. Finally, a rough estimation of the incremental apparent elastic modulus, as a function of strain, i.e., d*E*/dε, is identified. The compressive toughness W_c is determined as the sum of W_i toughness values calculated in the same strain-range $\Delta\varepsilon_i$. Relevant to the compressive strength and deformability of a material, compressive toughness reflects the property of absorbing energy and resisting damage when the material is under compressive damage. In particular, in this analysis, is determined the maximum energy that can be absorbed per unit volume without creating permanent deformations or irreversible damages.

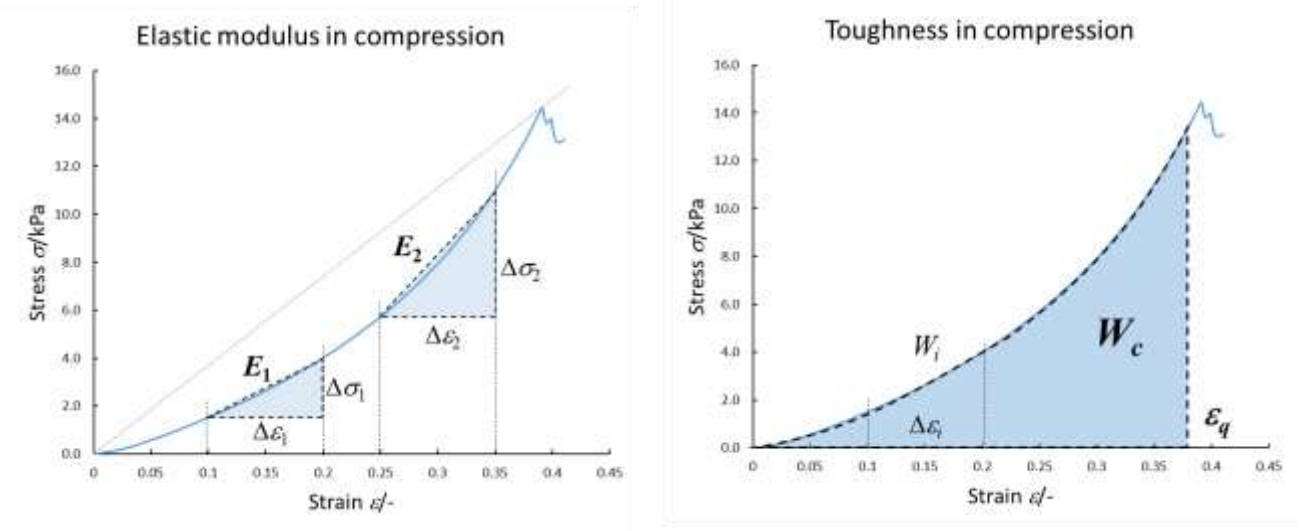

Figure 4. Stress-strain diagram until failure of a gel-based sample (exemplification on sample #3). apparent elastic modulus strain-range dependant and toughness in compression.

Within the stretched-elastic region, with the aim to identify possible deviations due to the viscoelastic behavior [70 – 72], and to guarantee the coupling between the sample and the plates, a series of hysteresis loops is performed, before reaching the breaking or yielding point. By way of example, the series of five compressions and five decompressions applied to gel-based sample #4, is shown in Figure 5.

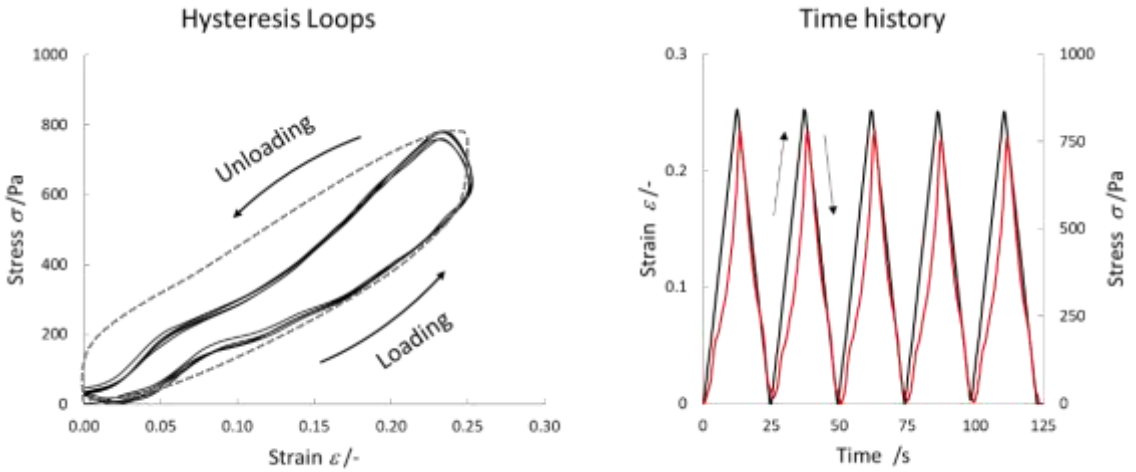

Figure 5. Hysteresis loops between 0 % and 25 % of strain (exemplification on sample #4) and the related time history (black line is the imposed strain and red line is the occurring stress).

As it is possible to notice, no significant degradation of elastic behavior occurs, i.e., the slopes are constant, and a full elastic recovery is achieved, as also shown in the graph of time history. This evidence allows verifying that stretched-elastic response is not affected by substantial losses of internal energy, during the deformation in compression.

3. Experimental results

The apparent elastic modulus E and the compressive toughness W_c of tissue engineering scaffolds have been determined in the stretched-elastic region, based on stress-strain experimental data. In practice, the elastic region is defined below the value of the yield strength, (identified as the value for which the second derivative of the stretched stress-strain curve nullifies), or before failure, depending on the inherent mechanical behavior. Within the same strain-range, the compressive toughness is determined as well. In Figures from 6 to 11, the complete stress-strain diagrams (up to failure) of the six gel-based samples tested in this work, are shown. The graphs also show the five pre-imposed hysteresis loops, performed to stabilize the sample between the plates and to identify any possible drift due to plastic deformations; and the extensibility value ε_q, within the stretched-elastic region, is considered as the upper limit for apparent elastic modulus and compressive toughness determination. In the Tables, the measured apparent elastic modulus E_i and toughness W_i average values, are reported within the corresponding strain ranges $\Delta\varepsilon$. Uncertainty values are calculated from reproducibility in quadruplicate.

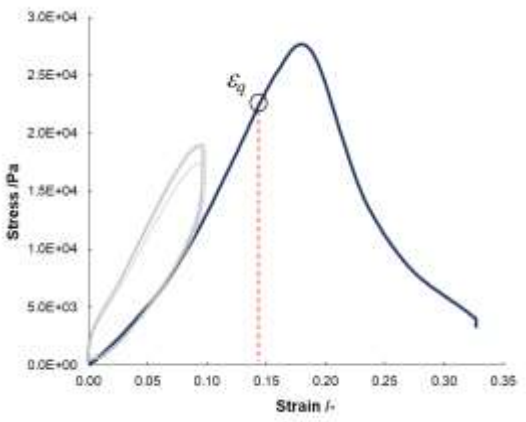

Strain range $\Delta\varepsilon_i$	Apparent elastic modulus E_i/kPa	Toughness W_c /kJ·m^{-3}
0 % - 5 %	103±9	0.12±0.003
5 % - 10 %	155±12	0.44±0.011
10 % - 15 %	212±18	0.91±0.024

Figure 6. Sample #1: Agar sample experimental stress-strain diagram. Apparent elastic modulus has been evaluated until 15 % in 3 steps of 5 % of strain.

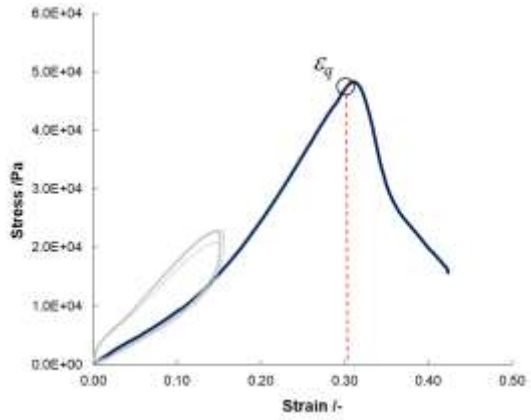

Strain range $\Delta\varepsilon_i$	Apparent elastic modulus E_i/kPa	Toughness W_c /kJ·m^{-3}
0 % - 5 %	89±10	0.11±0.004
5 % - 10 %	91±13	0.32±0.017
10 % - 15 %	132±16	0.61±0.020
15 % - 20 %	181±19	1.01±0.048
20 % - 25 %	224±25	1.48±0.053
25 % - 30 %	225±26	2.10±0.077

Figure 7. Sample #2: k-Carrageenan experimental stress-strain diagram. Apparent elastic modulus has been evaluated until 30 % in 6 steps of 5 % of strain.

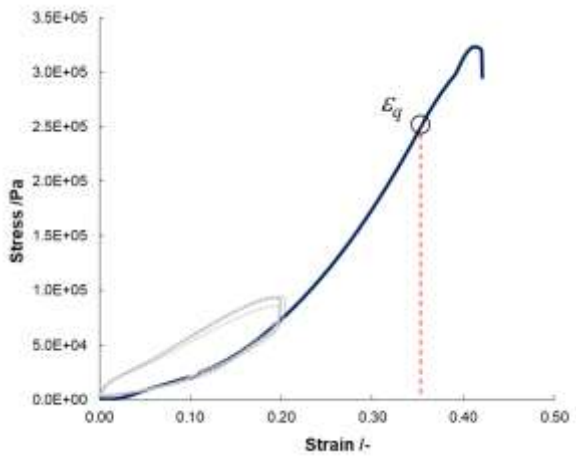

Strain range $\Delta\varepsilon_i$	Apparent elastic modulus E_i/kPa	Toughness W_c /kJ·m^{-3}
0 % - 5 %	205±26	0.25±0.012
5 % - 10 %	280±29	0.82±0.033
10 % - 15 %	528±55	1.92±0.055
15 % - 20 %	844±97	3.57±0.147
20 % - 25%	1150±155	5.80±0.373
25 % - 30 %	1480±186	8.63±0.351
30 % - 35 %	1490±226	12.1±0.681

Figure 8. Sample #3: Gellam Gum experimental stress-strain diagram. Apparent elastic modulus has been evaluated until 35 % in 7 steps of 5 % of strain.

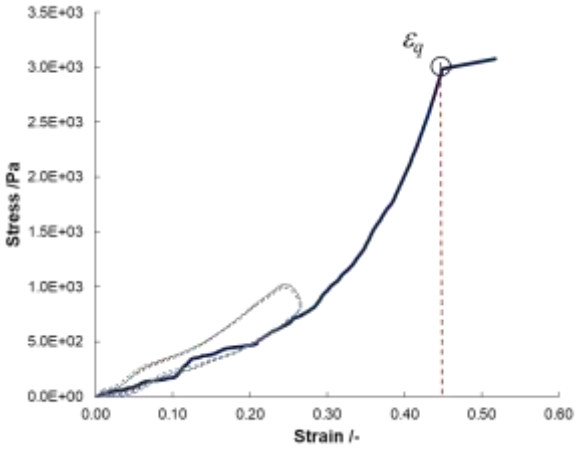

Strain range $\Delta\varepsilon_i$	Apparent elastic modulus E_i/kPa	Toughness W_c /kJ·m^{-3}
0 % - 5 %	3±0.5	0.002±0.001
5 % - 10 %	2±0.4	0.01±0.001
10 % - 15 %	5±0.9	0.02±0.001
15 % - 20 %	2±0.3	0.02±0.001
20 % - 25 %	4±0.7	0.03±0.002
25 % - 30 %	5±0.9	0.04±0.002
30 % - 35 %	8±1.4	0.06±0.004
35 % - 40 %	12±2.0	0.08±0.004
40 % - 45 %	20±3.5	0.12±0.005

Figure 9. Sample #4: Polyvinylalcohol, (PVA) experimental stress-strain diagram. Apparent elastic modulus has been evaluated until 45 % in 9 steps of 5 % of strain.

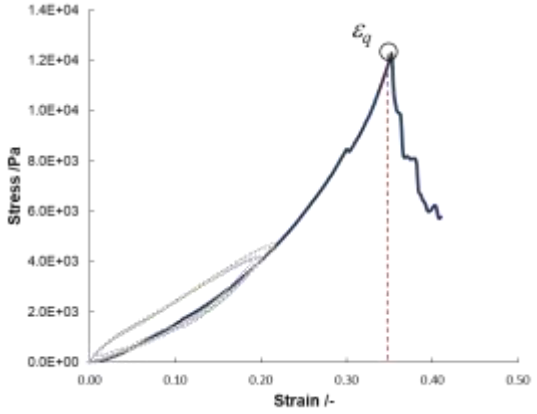

Strain range $\Delta\varepsilon_i$	Apparent elastic modulus E_i/kPa	Toughness W_c /kJ·m^{-3}
0 % - 5 %	10±1.4	0.01±0.001
5 % - 10 %	18±2.3	0.05±0.003
10 % - 15 %	21±3.5	0.10±0.003
15 % - 20 %	28±3.6	0.16±0.007
20 % - 25 %	36±5.3	0.25±0.019
25 % - 30 %	49±6.5	0.35±0.037
30 % - 35 %	67±10.4	0.50±0.036

Figure10. Sample #5: Polyacrylamide, PAA, with experimental stress-strain diagram. Apparent elastic modulus has been evaluated until 45 % in 7 steps of 5 % of strain.

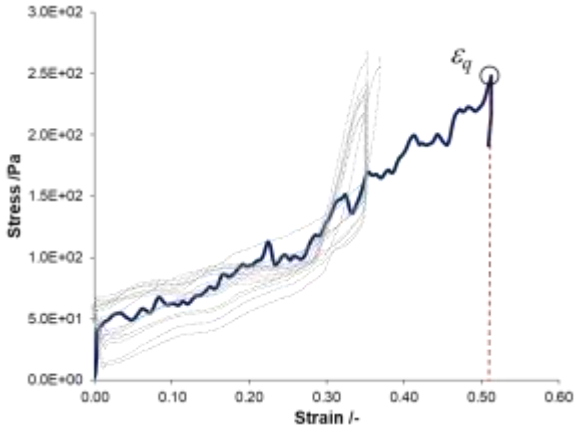

Strain range $\Delta\varepsilon_i$	Apparent elastic modulus E_i/kPa	Toughness W_c /kJ·m^{-3}
0 % - 10 %	0.33±0.06	0.005±0.001
10 % - 20 %	0.34±0.06	0.008±0.001
20 % - 30 %	0.49±0.09	0.01±0.001
30 % - 40 %	0.65±0.12	0.02±0.003
40 % - 50 %	0.65±0.12	0.02±0.003

Figure 11. Sample #6: ECM-gel, with experimental stress-strain diagram. Apparent elastic modulus has been evaluated until 50 % in 5 steps of 10 % of strain.

In the following Table 2 are summarized the values of yield stress and strain (ε_y and σ_y) and fracture stress and strain (ε_f and σ_f), from stress-strain experimental curves of the investigate gel-based samples. In the samples #1, #2 and #3, no yield occurs, since catastrophic failure.

Table 2. The yield stress and strain, and the fracture stress and strain of gel-based samples analyzed in this investigation.

Sample #	Yield strain ε_y /-	Yield stress σ_y /kPa	Fracture strain ε_f /-	Fracture stress σ_f /kPa
# 1	0.148	22.1	0.178	27.6
# 2	0.314	47.4	0.323	48.2
# 3	0.358	250	0.416	320
# 4	-	-	0.451	2.9
# 5	-	-	0.387	11.8
# 6	-	-	0.517	0.24

In Table 3 are summarized the basic functional attributes of investigate gel-based samples, in terms of apparent elastic modulus E, ranging in the related stretched elastic regions within the strain limits $0 \leq \varepsilon \leq \varepsilon_q$, the corresponding incremental apparent elastic modulus $dE/d\varepsilon$, and the compressive toughness W_c. The values of extensibility ε_q (at the strength σ_q) correspond to yield strain ε_y or to fracture strain ε_f, depending on the observed mechanical behavior. The incremental apparent elastic modulus quantifies the degree of stretched elastic slope: high values indicate strong nonlinearity, on the contrary, if the elastic response tends to be linear, the incremental apparent elastic modulus tends to 0. Experimental results shown in Table 2 are expressed as average values: measurement uncertainty can be considered negligible (below 2 %), with respect to the material variability, ranging from 10 % up to 20 %, determined from reproducibility in quadruplicate, as shown in tables of Figures 6-11.

Table 3. The functional mechanical attributes of gel-based samples analyzed in this investigation.

Sample #	Extensibility Strain upper limit ε_q /-	Strength Stress upper limit σ_q /kPa	Range of apparent elastic modulus E /kPa	Incremental apparent elastic modulus $dE/d\varepsilon$ /kPa	Toughness W_c /kJ·m^{-3}
# 1	ε_y=0.148	22.1	100 – 210	~1000	1.47
# 2	ε_y=0.314	47.4	90 – 230	~900	5.62
# 3	ε_y=0.358	250	200 – 1500	~6000	33.1
# 4	ε_b=0.451	2.9	2 – 20	~35	0.38
# 5	ε_b=0.387	11.8	10 – 80	~180	2.03
# 6	ε_b=0.517	0.24	0.3 – 0.7	~0.95	0.06

4. Discussion and conclusion

The apparent elastic modulus in compression E and the compressive toughness W_c of six gel-based tissue engineering scaffolds have been determined in the stretched-elastic region, based on stress-strain experimental results. The polymeric matrices of molded tissue-engineering gel-based scaffolds are polysaccharides, synthetic polymers, and Extracellular matrix. Strictly speaking, the increasing values of apparent elastic modulus in compression, here estimated as a function of discrete intervals of applied strain range, relies to strain-stiffening effect, as a sudden increase of the apparent elastic modulus under strain. The proposed segmentation of the non-linear curve (up to a definition of the incremental apparent elastic modulus), allows to minimize the differential between secant and curve below, up to define an average elastic response of the investigated gel-based scaffold subjected to compression strain, in terms apparent elastic modulus, as a function of strain ranges.

The knowledge of the variation of the apparent elastic modulus of a gel-based scaffolds in tissue engineering, as a function of strain range, allows to better define the elastic response for many applicative and engineering working condition, both in vitro and in vivo, in which variable deformations (or stress) can occur, and it is useful for improve the accuracy of computational models and simulations.

The measurements aimed at evaluating the stress-strain behavior up to breaking point, by identifying yield or breaking strain, and the related elastic region: from the slope of the stress-strain curve, as a function of different steps of strain-ranges, the values of apparent elastic modulus strain-range dependent E_i, is determined from relation (1); the toughness in compression W_c is determined by calculating the area under the stress-strain curve, from relation (2), based on a cubic polynomial function, relation (3). Since investigations are inherent to elastic behavior, a series of pre-imposed hysteresis loops are performed to identify and prevent possible drifts due to plastic deformations.

As shown in the graphs of Figures from 6 to 11, the mechanical behavior of examined gel-based scaffolds, narrowly mimics native human tissue behavior in compression, since a typical exponential incremental stress-strain curve occurs; as a consequence, due to the non-linear elastic behavior of this kind of materials, apparent elastic modulus has to be expressed as a function of the related strain-range (beyond temperature, strain-rate, and applied stress), to accurately assess the actual mechanical

response of occurring deformations. As observed, apparent elastic modulus E tends to increase by increasing the imposed deformation $\Delta\varepsilon$ (instead of keeping constant), thus a rough estimation of the incremental apparent elastic modulus, $dE/d\varepsilon$, can be identified for each sample, within the whole examined strain range, from 0 up to ε_q. By considering these ranges of elastic response and mechanical behavior, the experimental data of apparent elastic modulus can be considered closely representative of several native soft human tissues, as shown below in Figure 12.

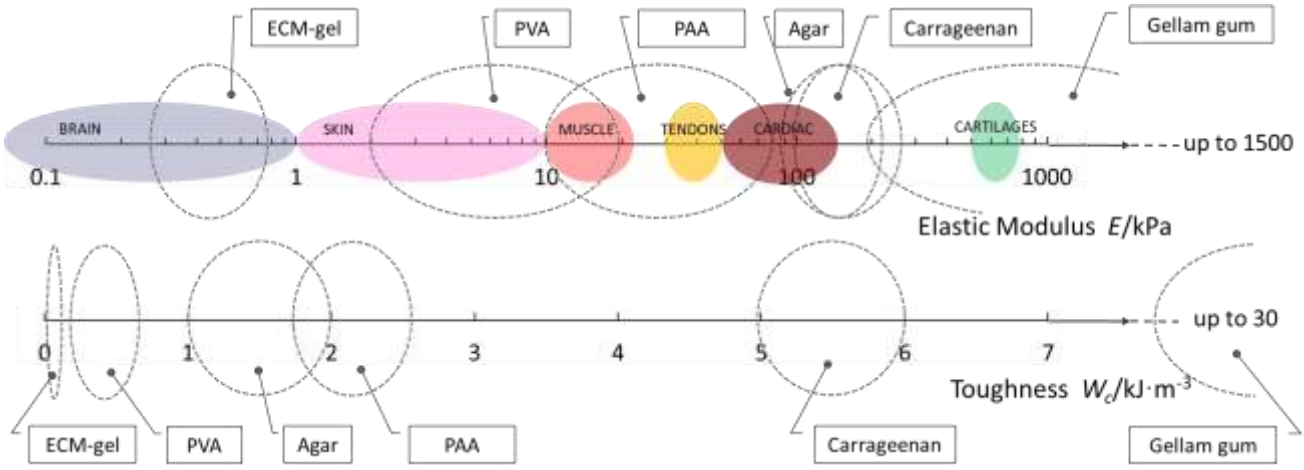

Figure 12. Apparent elastic modulus compared with native soft human tissues, and compressive toughness of investigated gel-based samples.

The apparent elastic behavior of ECM-gel is compatible with brain tissues, PVA with skin and muscle, PAA with muscle, tendon, and cardiac tissues, Agar and Carrageenan with cardiac tissues, and Gellam gum with cartilages. Compressive toughness gives information about the aptitude of absorbing energy and resisting damage under compression. In particular, is identified the maximum energy that can be absorbed by the gel before permanent deformations or irreversible damages, i.e., a quantitative range of workability. In terms of compressive toughness, Gellam gum ~30 kJ·m^{-3} and Carrageenan ~6 kJ·m^{-3}, show a very high aptitude of resisting damage under compression; PAA, between ~2 kJ·m^{-3} and ~3 kJ·m^{-3}, and Agar ranging between ~1 kJ·m^{-3} and ~2 kJ·m^{-3}, show good workability, while PVA ~0.4 kJ·m^{-3} and ECM-gel < 0.1 kJ·m^{-3} show a limited range of workability, before failure or plastic deformation.

5. References

[1] Nezhad-Mokhtari, P., Ghorbani, M., Roshangar, L., & Rad, J. S. (2019). A review on the construction of hydrogel scaffolds by various chemically techniques for tissue engineering. European Polymer Journal, 117, 64-76.

[2] Spicer, C. D. (2020). Hydrogel scaffolds for tissue engineering: the importance of polymer choice. Polymer Chemistry, 11(2), 184-219.

[3] Taghipour, Y. D., Hokmabad, V. R., Bakhshayesh, D., Rahmani, A., Asadi, N., Salehi, R., & Nasrabadi, H. T. (2020). The application of hydrogels based on natural polymers for tissue engineering. Current medicinal chemistry.

[4] Dhandayuthapani, B., Yoshida, Y., Maekawa, T., & Kumar, D. S. (2011). Polymeric scaffolds in tissue engineering application: a review. International journal of polymer science, 2011.

[5] Van Vlierberghe, S., Dubruel, P., & Schacht, E. (2011). Biopolymer-based hydrogels as scaffolds for tissue engineering applications: a review. Biomacromolecules, 12(5), 1387-1408.

[6] Utech, S., & Boccaccini, A. R. (2016). A review of hydrogel-based composites for biomedical applications: enhancement of hydrogel properties by addition of rigid inorganic fillers. Journal of materials science, 51(1), 271-310.

[7] Drury, Jeanie L., and David J. Mooney. "Hydrogels for tissue engineering: scaffold design variables and applications." Biomaterials 24.24 (2003): 4337-4351.

[8] Loh, Q. L., & Choong, C. (2013). Three-dimensional scaffolds for tissue engineering applications: role of porosity and pore size. Tissue Engineering Part B: Reviews, 19(6), 485-502.

[9] Markert, C. D., Guo, X., Skardal, A., Wang, Z., Bharadwaj, S., Zhang, Y., ... & Guthold, M. (2013). Characterizing the micro-scale elastic modulus of hydrogels for use in regenerative medicine. journal of the mechanical behavior of biomedical materials, 27, 115-127.

[10] Gurkan, U. A., Tasoglu, S., Kavaz, D., Demirel, M. C., & Demirci, U. (2012). Emerging technologies for assembly of microscale hydrogels. Advanced healthcare materials, 1(2), 149-158.

[11] Leijten, J., Rouwkema, J., Zhang, Y. S., Nasajpour, A., Dokmeci, M. R., & Khademhosseini, A. (2016). Advancing Tissue Engineering: A Tale of Nano-, Micro-, and Macroscale Integration. Small, 12(16), 2130-2145.

[12] Ozbolat, I. T. (2015). Bioprinting scale-up tissue and organ constructs for transplantation. Trends in biotechnology, 33(7), 395-400.

[13] Selvan, N. K., Shanmugarajan, T. S., & Uppuluri, V. N. V. A. (2020). Hydrogel based scaffolding polymeric biomaterials: Approaches towards skin tissue regeneration. Journal of Drug Delivery Science and Technology, 55, 101456.

[14] Chuah, Y. J., Peck, Y., Lau, J. E. J., Hee, H. T., & Wang, D. A. (2017). Hydrogel based cartilaginous tissue regeneration: recent insights and technologies. Biomaterials science, 5(4), 613-631.

[15] Sun, Z., Song, C., Wang, C., Hu, Y., & Wu, J. (2019). Hydrogel-based controlled drug delivery for cancer treatment: a review. Molecular Pharmaceutics, 17(2), 373-391.

[16] He, D., Zhao, A. S., Su, H., Zhang, Y., Wang, Y. N., Luo, D., ... & Yang, P. (2019). An injectable scaffold based on temperature-responsive hydrogel and factor-loaded nanoparticles for application in vascularization in tissue engineering. Journal of Biomedical Materials Research Part A, 107(10), 2123-2134.

[17] Moraes, T. B. F., Politi, M. J., & Triboni, E. R. (2019). Application and Perspectives. In Nano Design for Smart Gels (pp. 207-237). Elsevier.

[18] Hong, Y., Zhou, F., Hua, Y., Zhang, X., Ni, C., Pan, D., ... & Zou, Y. (2019). A strongly adhesive hemostatic hydrogel for the repair of arterial and heart bleeds. Nature communications, 10(1), 1-11.

[19] Op't Veld, R. C., Walboomers, X. F., Jansen, J. A., & Wagener, F. A. (2020). Design Considerations for Hydrogel Wound Dressings: Strategic and Molecular Advances. Tissue Engineering Part B: Reviews.

[20] Zhu, T., Mao, J., Cheng, Y., Liu, H., Lv, L., Ge, M., ... & Yang, L. (2019). Recent Progress of Polysaccharide-Based Hydrogel Interfaces for Wound Healing and Tissue Engineering. Advanced Materials Interfaces, 6(17), 1900761.

[21] Mitura, S., Sionkowska, A., & Jaiswal, A. (2020). Biopolymers for hydrogels in cosmetics. Journal of Materials Science: Materials in Medicine, 31, 1-14.

[22] Cascone, S., & Lamberti, G. (2020). Hydrogel-based commercial products for biomedical applications: A review. International Journal of Pharmaceutics, 573, 118803.

[23] Zagórska-Dziok, M., & Sobczak, M. (2020). Hydrogel-Based Active Substance Release Systems for Cosmetology and Dermatology Application: A Review. Pharmaceutics, 12(5), 396.

[24] Basinger, B.C., Rowley, A.P., Chen,K., Humayun, M.S., Weiland, J. D., 2009. Finite element modelling of retinal prosthesis mechanics. J. Neural Eng.6 (5),055006.

[25] Colodetti, L., Weiland,J.D., Colodetti,A., Ray,A., Seiler,M.J., Hinton, D.R., Humayun, M.S.,2007. Pathology of damaging electrical stimulation in the retina. Exp. Eye Res.85,23–33.

[26] Franke,O., Durst,K., Maier,V., Goken, M., Birkholz, T., Schneider, H., Hennig, F., Gelse, K., 2007.Mechanical properties of hyaline and repair cartilage studied by nanoindentation. Acta Biomater. 3,873–881.

[27] Verma, V., Verman, P., Kar, S., Ray, P., Ray, A.R., 2006. Fabrication of agar–gelatin hybrid scaffolds using a novel entrapment method for in vitro tissue engineering applications. Biotechnol. Bioeng. 96, 392–400.

[28] Dave, P.C., Dingal, P., Discher, D.E., 2014. Material control of stem cell differentiation: challenges in nano-characterization. Curr. Opin. Biotechnol.28,46–50.

[29] Akiki, R. K., & Mehrzad, R. (2020). Practical management of common skin injuries, lacerations, wounds, trigger fingers, and burns. The Journal of the American Board of Family Medicine, 33(5), 799-808.

[30] Marwan, H., Sawatari, Y., & Peleg, M. (2020). Soft Tissue Management in Orbital-Zygomaticomaxillary Surgery. In Management of Orbito-zygomaticomaxillary Fractures (pp. 63-71). Springer, Cham.

[31] Cui, N., Han, K., Zhou, C., Seong, M., Lu, T., & Jeong, H. E. (2020). A Tough Polysaccharide-Based Hydrogel with an On-Demand Dissolution Feature for Chronic Wound Care through Light-Induced Ultrafast Degradation. ACS Applied Bio Materials.

[32] Arain, A. R., Cole, K., Sullivan, C., Banerjee, S., Kazley, J., & Uhl, R. L. (2018). Tissue expanders with a focus on extremity reconstruction. Expert Review of Medical Devices, 15(2), 145-155.

[33] Jaspers, M., Dennison, M., Mabesoone, M. F., MacKintosh, F. C., Rowan, A. E., Kouwer, P. H. (2014). Ultra-responsive soft matter from strain-stiffening hydrogels. Nature communications, 5(1), 1-8.

[34] Storm, C., Pastore, J. J., MacKintosh, F. C., Lubensky, T. C., Janmey, P. A. (2005). Nonlinear elasticity in biological gels. Nature, 435(7039), 191-194.

[35] Fischenich, K. M., Lewis, J. T., Bailey, T. S., & Donahue, T. L. H. (2018). Mechanical viability of a thermoplastic elastomer hydrogel as a soft tissue replacement material. Journal of the mechanical behavior of biomedical materials, 79, 341-347.

[36] Gombert, Y., Simič, R., Roncoroni, F., Dübner, M., Geue, T., & Spencer, N. D. (2019). Structuring hydrogel surfaces for tribology. Advanced Materials Interfaces, 6(22), 1901320.

[37] Kingsley, D. M., McCleery, C. H., Johnson, C. D., Bramson, M. T., Rende, D., Gilbert, R. J., & Corr, D. T. (2019). Multi-modal characterization of polymeric gels to determine the influence of testing method on observed elastic modulus. Journal of the mechanical behavior of biomedical materials, 92, 152-161.

[38] Schiavi, A., Cuccaro, R., & Troia, A. (2016). Strain-rate and temperature dependent material properties of Agar and Gellan Gum used in biomedical applications. Journal of the mechanical behavior of biomedical materials, 53, 119-130.

[39] Bozler, E. (1936, January). An analysis of the properties of smooth muscle. In Cold Spring Harbor Symposia on Quantitative Biology (Vol. 4, pp. 260-266). Cold Spring Harbor Laboratory Press.

[40] Fung, Y. C. (1967). Elasticity of soft tissues in simple elongation. American Journal of Physiology-Legacy Content, 213(6), 1532-1544.

[41] Larrabee Jr, W. F. (1986). A finite element model of skin deformation. I. Biomechanics of skin and soft tissue: a review. The Laryngoscope, 96(4), 399-405.

[42] Larrabee Jr, W. F., & Sutton, D. (1986). A finite element model of skin deformation. II. An experimental model of skin deformation. The Laryngoscope, 96(4), 406-412.

[43] Griffin, M., Premakumar, Y., Seifalian, A., Butler, P. E., & Szarko, M. (2016). Biomechanical characterization of human soft tissues using indentation and tensile testing. JoVE (Journal of Visualized Experiments), (118), e54872.

[44] Morales-Orcajo, E., de Bengoa Vallejo, R. B., Iglesias, M. L., & Bayod, J. (2016). Structural and material properties of human foot tendons. Clinical Biomechanics, 37, 1-6.

[45] Kalra, A., Lowe, A., & Al-Jumaily, A. M. (2016). Mechanical behaviour of skin: a review. J. Mater. Sci. Eng, 5(4), 1000254.

[46] Karimi, A., Shojaei, A., & Tehrani, P. (2017). Mechanical properties of the human spinal cord under the compressive loading. Journal of chemical neuroanatomy, 86, 15-18.

[47] Alekya, B., Rao, S., & Pandya, H. J. (2019). Engineering approaches for characterizing soft tissue mechanical properties: A review. Clinical Biomechanics, 69, 127-140.

[48] Kranjec, M., Trajkovski, A., Krašna, S., Hribernik, M., & Kunc, R. (2020). Material properties of human patellar-ligament grafts from the elderly population. Journal of the Mechanical Behavior of Biomedical Materials, 110, 103994.

[49] Gosline, J., Lillie, M., Carrington, E., Guerette, P., Ortlepp, C., & Savage, K. (2002). Elastic proteins: biological roles and mechanical properties. Philosophical Transactions of the Royal Society of London. Series B: Biological Sciences, 357(1418), 121-132.

[50] Liu, J., Zheng, H., Poh, P. S., Machens, H. G., & Schilling, A. F. (2015). Hydrogels for engineering of perfusable vascular networks. International journal of molecular sciences, 16(7), 15997-16016.

[51] Salati, M. A., Khazai, J., Tahmuri, A. M., Samadi, A., Taghizadeh, A., Taghizadeh, M., ... & Saeb, M. R. (2020). Agarose-Based Biomaterials: Opportunities and Challenges in Cartilage Tissue Engineering. Polymers, 12(5), 1150.

[52] Anjum, Fraz, et al. "Tough, semisynthetic hydrogels for adipose derived stem cell delivery for chondral defect repair." Macromolecular bioscience 17.5 (2017): 1600373.

[53] Su, Teng, et al. "Strong bioinspired polymer hydrogel with tunable stiffness and toughness for mimicking the extracellular matrix." ACS Macro Letters 5.11 (2016): 1217-1221.

[54] Latifi, N., Asgari, M., Vali, H., & Mongeau, L. (2018). A tissue-mimetic nano-fibrillar hybrid injectable hydrogel for potential soft tissue engineering applications. Scientific reports, 8(1), 1-18.

[55] Ni, Y., Tang, Z., Cao, W., Lin, H., Fan, Y., Guo, L., & Zhang, X. (2015). Tough and elastic hydrogel of hyaluronic acid and chondroitin sulfate as potential cell scaffold materials. International journal of biological macromolecules, 74, 367-375.

[56] Drozdov, A. D., & Christiansen, J. D. (2020). Tension–compression asymmetry in the mechanical response of hydrogels. Journal of the Mechanical Behavior of Biomedical Materials, 110, 103851.

[57] Chen, C., Tang, J., Gu, Y., Liu, L., Liu, X., Deng, L., ... & Chen, L. (2019). Bioinspired hydrogel electrospun fibers for spinal cord regeneration. Advanced Functional Materials, 29(4), 1806899.

[58] Che, L., Lei, Z., Wu, P., & Song, D. (2019). A 3d printable and bioactive hydrogel scaffold to treat traumatic brain injury. Advanced Functional Materials, 29(39), 1904450.

[59] Gao, F., Xu, Z., Liang, Q., Li, H., Peng, L., Wu, M., ... & Liu, W. (2019). Osteochondral Regeneration with 3D-Printed Biodegradable High-Strength Supramolecular Polymer Reinforced-Gelatin Hydrogel Scaffolds. Advanced Science, 6(15), 1900867.

[60] Almany, L., & Seliktar, D. (2005). Biosynthetic hydrogel scaffolds made from fibrinogen and polyethylene glycol for 3D cell cultures. Biomaterials, 26(15), 2467-2477.

[61] Dorishetty, P., Balu, R., Athukoralalage, S. S., Greaves, T. L., Mata, J., De Campo, L., ... & Choudhury, N. R. (2020). Tunable biomimetic hydrogels from silk fibroin and nanocellulose. ACS Sustainable Chemistry & Engineering, 8(6), 2375-2389.

[62] Distler, T., Schaller, E., Steinmann, P., Boccaccini, A. R., & Budday, S. (2020). Alginate-based hydrogels show the same complex mechanical behavior as brain tissue. Journal of the Mechanical Behavior of Biomedical Materials, 111, 103979.

[63] Kozlowska, J., Pauter, K., & Sionkowska, A. (2018). Carrageenan-based hydrogels: Effect of sorbitol and glycerin on the stability, swelling and mechanical properties. Polymer Testing, 67, 7-11.

[64] Bonifacio, M. A., Gentile, P., Ferreira, A. M., Cometa, S., & De Giglio, E. (2017). Insight into halloysite nanotubes-loaded gellan gum hydrogels for soft tissue engineering applications. Carbohydrate polymers, 163, 280-291.

[65] Charron, P. N., Braddish, T. A., & Oldinski, R. A. (2019). PVA-gelatin hydrogels formed using combined theta-gel and cryo-gel fabrication techniques. Journal of the mechanical behavior of biomedical materials, 92, 90-96.

[66] Buyanov, A. L., Gofman, I. V., & Saprykina, N. N. (2019). High-strength cellulose–polyacrylamide hydrogels: mechanical behavior and structure depending on the type of cellulose. Journal of the mechanical behavior of biomedical materials, 100, 103385.

[67] Choi S. H., Kim Y. H., Hebisch M., Sliwinski C., Lee S., D'Avanzo C., Klee J. B., A three-dimensional human neural cell culture model of Alzheimer's disease, Nature, 515 (2014), pp. 274-278.

[68] Zhang, Junhua, Christopher R. Daubert, and E. Allen Foegeding. "Characterization of polyacrylamide gels as an elastic model for food gels." Rheologica acta 44.6 (2005): 622-630.

[69] Jeong, C. G., & Hollister, S. J. (2010). Mechanical, permeability, and degradation properties of 3D designed poly (1, 8 octanediol-co-citrate) scaffolds for soft tissue engineering. Journal of Biomedical Materials Research Part B: Applied Biomaterials: An Official Journal of The Society for Biomaterials, The Japanese Society for Biomaterials, and The Australian Society for Biomaterials and the Korean Society for Biomaterials, 93(1), 141-149.

[70] Schiavi, A., & Prato, A. (2017). Evidences of non-linear short-term stress relaxation in polymers. Polymer Testing, 59, 220-229.

[71] Cacopardo, L., Guazzelli, N., Nossa, R., Mattei, G., & Ahluwalia, A. (2019). Engineering hydrogel viscoelasticity. Journal of the mechanical behavior of biomedical materials, 89, 162-167.

[72] Cacopardo, L., Mattei, G., & Ahluwalia, A. (2020). A new load-controlled testing method for viscoelastic characterisation through stress-rate measurements. Materialia, 9, 100552.